ARTICLE

INTERNATIONAL JOURNAL OF
CHEMICAL KINETICS WILEY

Main sources of uncertainty in recent methanol/NOx combustion models

Márton Kovács [ID] | **Máté Papp** [ID] | **István Gy. Zsély** [ID] | **Tamás Turányi** [ID]

Department of Physical Chemistry, Institute of Chemistry, ELTE Eötvös Loránd University, Budapest, Hungary

Correspondence
István Gy. Zsély, Department of Physical Chemistry, Institute of Chemistry, ELTE Eötvös Loránd University, 1117 Budapest, Pázmány Péter sétány 1/A, Hungary.
Email: zsigy@chem.elte.hu

Abstract

The performance of 17 recent detailed reaction mechanisms describing the interactions of methanol and formaldehyde with nitrogen oxides in combustion systems was investigated based on large number of literature experimental data covering a wide range of conditions. This data collection consists of 2552 data points of concentration profiles in 243 datasets measured in jet stirred reactors, tubular flow reactors, and shock tubes. The two best mechanisms were found to be the Shrestha-2019 and Glarborg-2018 mechanisms, which were selected for further investigations. Two additional mechanisms were created via the replacement of the hydrogen, syngas, methanol submechanisms, and the parameters of nine N/H/O reactions to ones from our previous mechanism optimization studies. Local sensitivity analysis of the kinetic and thermodynamic parameters (Arrhenius A-factors, heat capacities, standard enthalpies of formation, and standard molar entropies) of these four mechanisms was carried out. The results were in good agreement and the most sensitive reactions belong to the neat hydrogen, syngas, or methanol oxidation. The most important reactions of the interaction between C_1 species and NOx are hydrogen-abstraction reactions $CH_3OH + NO_2 = HONO + CH_2OH$ and $CH_2O + NO_2 = HONO + HCO$. The most sensitive thermodynamic properties are the molar heat capacities of species OH, NO, HONO, and NO_2, and the standard enthalpies of formation and entropies of these species have also significant sensitivities. According to the local uncertainty analysis of the kinetic and thermodynamic parameters, the rate coefficients of the NOx chemistry have the highest contribution to the overall uncertainty of the simulation results, especially those of the two reactions above. The highest uncertainty caused by the thermodynamic parameters is due to the heat capacity of HNO, OH, HO_2, and NO_2 and some other species, whereas the uncertainty contributions of all enthalpies of formation and entropies were negligible.

KEYWORDS
mechanism comparison, methanol combustion, NOx chemistry, sensitivity analysis, uncertainty analysis

1 | INTRODUCTION

One of the important tasks today is to reduce the usage of fossil transportation fuels, and alcohols are promising alternative fuels. The reactions of nitrogen oxides in combustion systems are also important due to environmental regulations. Nevertheless, compared with CH_4/NOx systems, much less literature measurement data are available to describe the interaction of methanol and nitrogen compounds in combustion systems. These measurements show that the presence of NO and NO_2, even in trace amounts, significantly affects the oxidation of methanol. Several detailed reaction mechanisms were published in the last decades to describe methanol combustion with complete pathways for NOx reactions included but the simulation results still have high uncertainty.

The performance of a mechanism can be improved with a more accurate determination of the most important rate parameters and thermodynamic data. One possible approach is to carry out new direct measurements or theoretical calculations for the determination of the key parameters with low uncertainty. Another approach is to do mechanism optimization[1–8] by fitting the parameters within their uncertainty limits to the results of direct and indirect measurements and theoretical determinations. In both cases, the first step is the identification of those parameters of the chemical kinetic models that cause the largest uncertainty of the model results of interest.

In this work, experiments in homogeneous reactors on methanol–oxygen combustion systems doped with NO or NO_2 were considered. The measurements include concentration profiles measured in jet stirred reactors (JSRs), tubular flow reactors (TFRs), and shock tubes (STs). The performance of three recent combustion simulation solvers, FlameMaster 4.2.1,[9] FlameMaster 4.0.0,[10] and OpenSMOKE++ 0.12.0,[11,12] was also tested and compared. These three programs gave almost identical results in most cases. The main article contains the results obtained with OpenSMOKE++, whereas the detailed comparison of the results from the three solvers can be found in the Supplementary Material, Part 1.

The performance of 17 recent detailed mechanisms was tested on the simulation of the collected methanol/NOx or formaldehyde/NOx experiments. Then, local sensitivity and uncertainty analyses of the best mechanisms were carried out. The results highlighted the main sources of uncertainty in the modeling of methanol/NOx systems.

2 | COLLECTION OF EXPERIMENTAL DATA

The effects of nitrogen oxides on methanol and formaldehyde combustion have been investigated by several research groups using various experimental methods. Our aim was to collect all experimental data on methanol and formaldehyde combustion influenced with nitrogen oxides related to measurements in homogeneous reactors. The combustion of methanol perturbed with NOx have not been investigated in flames to our knowledge. Table 1 summarizes experimental conditions of the collected data points. All the related experiments were concentration profile measurements carried out in JSRs, TFRs, and STs.

All collected indirect experimental data (2552 data points in 243 datasets) were stored in 74 data files using the ReSpecTh Kinetics Data (RKD) Format Specification v2.3.[27] The RKD format was developed from the PrIMe Kinetics Data Format[28] by adding several new keywords and carrying out further modifications. The RKD-format XML files are well readable by both humans and computer codes. The RKD-format files were created with our in-house developed Optima++ code.[29] Optima++ was also used for reading the data files, running the FlameMaster or OpenSMOKE++ simulation codes, and comparing the simulation results with the experimental data.

We have estimated the standard deviation σ of the experimental data for each dataset. For this, we have calculated the square root of the sum of the square of the published or estimated experimental errors and the mean-square deviation of the data points from a fitted trend line. The trend line was obtained by spline or polynomial fitting using computer code Minimal Spline Fit.[30] The exact procedure for the estimation of the σ values is available in the Supplementary Material, Part 1 of article.[8] Tables S1 to S3 of the Supplementary Material, Part 1 of this article contain the estimated standard deviations of the experimental data. The RKD-format XML data files created for this work are available in the ReSpecTh information site.[31] This site also contains the latest version of the Optima++ code.

3 | COMPARISON OF THE MECHANISMS

The experimental data were reproduced using detailed reaction mechanisms developed for the description of NOx chemistry in combustion systems and had been widely used in science and industry. Some of them have not been validated to simulate methanol combustion or just at specific experimental conditions but were also tested here to see their performance on this system as the good performance of a mechanism out of its validation range has been observed several times. The footnotes of Table 2 summarize the validation background of the investigated mechanisms. Seventeen mechanisms were considered, which included the latest ones and several other mechanisms from the last

TABLE 1 Collected experimental concentration-profile data on CH$_3$OH/NOx measurements

Experiment type	Datasets	Data points	T (K)	p (atm)	φ
Jet stirred reactor (JSR)[13–15]	72	765	640–1870	0.92–10	0.3–1.34
Tubular flow reactor (TFR)[16–25]	160	1648	298–1420	0.99–1.4	0.01–13.5
Shock tube (ST)[26]	11	139	1142–1502	0.46–0.66	0.46–2
Overall	243	2552	298–1870	0.46–10	0.01–13.5

TABLE 2 Comparison of the error function values of the mechanisms for homogenous reactors with different experiment types

	Ref.	JSR 65 (689)	TFR 149 (1545)	ST 11 (139)	Overall 225 (2373)
Shrestha-2019[a]	32	27.3 (689)	16.4 (1545)	29.7 (139)	20.2 (2373)
Glarborg-2018[a]	33	22.2 (689)	36.8 (1545)	10.2 (139)	31.3 (2373)
GDFKin3.0-2016[c]	34	29.7 (689)	30.5 (1486)	65.9 (139)	32.1 (2314)
POLIMI-2014[a]	35	30.8 (689)	37.9 (1545)	32.4 (139)	35.5 (2373)
POLIMI-2019[b]	36	26.1 (689)	41.8 (1545)	56.2 (139)	37.9 (2373)
Rasmussen-2008[b]	16	48.7 (689)	40.8 (1486)	10.4 (139)	41.7 (2314)
Zaragoza-2016[c]	37	60.1 (689)	37.8 (1486)	10.2 (139)	43.2 (2314)
Saxena-2007[b]	38	20.8 (598)	38.6 (1535)	230.1 (139)	43.6 (2272)
Tian-2009[c]	39	47.6 (689)	46.7 (1486)	41.0 (139)	46.7 (2314)
AAU-2008[a]	40	30.1 (689)	55.2 (1486)	128.6 (139)	51.3 (2314)
SanDiego-2014[c]	41	48.4 (541)	41.4 (1535)	229.3 (139)	53.0 (2215)
Alzueta-2001[b]	19	53.4 (653)	57.5 (1486)	9.7 (139)	53.8 (2278)
Konnov-2009[a]	42	36.6 (479)	53.6 (1486)	157.7 (139)	55.4 (2104)
Aranda-2013[b]	43	28.6 (689)	70.2 (1496)	36.3 (139)	55.9 (2324)
Zaragoza-2011[c]	44	55.5 (689)	61.4 (1486)	8.8 (139)	56.9 (2314)
GRI3.0-1999[d]	45	32.8 (689)	107.7 (1486)	149.1 (139)	87.0 (2314)
Marques-2009[c]	46	172.5 (689)	188.4 (1486)	– (0)	183.3 (2175)
ELTE+Shrestha[a]	text	21.3 (689)	31.3 (1545)	8.5 (139)	27.3 (2373)
ELTE+Glarborg[a]	text	22.0 (689)	30.7 (1545)	14.6 (139)	27.4 (2373)

The number of the data points with successful simulation are given in parenthesis. The overall numbers of the datasets and data points of a group is summarized in the header of the table.

[a]The mechanism was developed to describe a wide range of experimental conditions and it was validated to simulate CH$_3$OH/NOx systems.

[b]The mechanism was developed to describe specific experimental conditions and it was validated to simulate CH$_3$OH/NOx systems.

[c]The mechanism was developed to describe specific experimental conditions and it was not validated to simulate CH$_3$OH/NOx systems. However, it contained the main corresponding routes, so its performance was tested.

[d]The mechanism was developed to describe a wide range of experimental conditions but it was not validated and supposed to be used to simulate methanol combustion or the CH$_3$OH/NOx chemical system. However, it contained the main corresponding routes, so its performance was also tested.

two decades. All collected experimental data were simulated with each of the mechanisms.

Agreement of the simulation results with the experimental data was investigated using the following error function.[7]

$$E(p) = \frac{1}{N} \sum_{i=1}^{N} \frac{1}{N_i} \sum_{j=1}^{N_i} \left(\frac{y_{ij}^{mod}(p) - y_{ij}^{exp}}{\sigma\left(y_{ij}^{exp}\right)} \right)^2 \qquad (1)$$

Here, N is the number of datasets and N_i is the number of data points in the i-th dataset. Vector $\boldsymbol{p}$ contains

the rate parameters. Values y_{ij}^{exp} and $\sigma(y_{ij}^{exp})$ are the j-th data point and its standard deviation, respectively, in the i-th dataset. The corresponding simulated (modeled) value is y_{ij}^{mod} obtained from a simulation using a detailed mechanism and an appropriate simulation method. The calculated error function value is a suitable quantitative measure to characterize the performance of a mechanism in a wide range of experimental conditions. The order according to the goodness of the mechanisms can be given based on this value and the actual best mechanism can be chosen. One can note that $E < 9$ means the mechanism can reproduce the experimental data within 3 sigma on
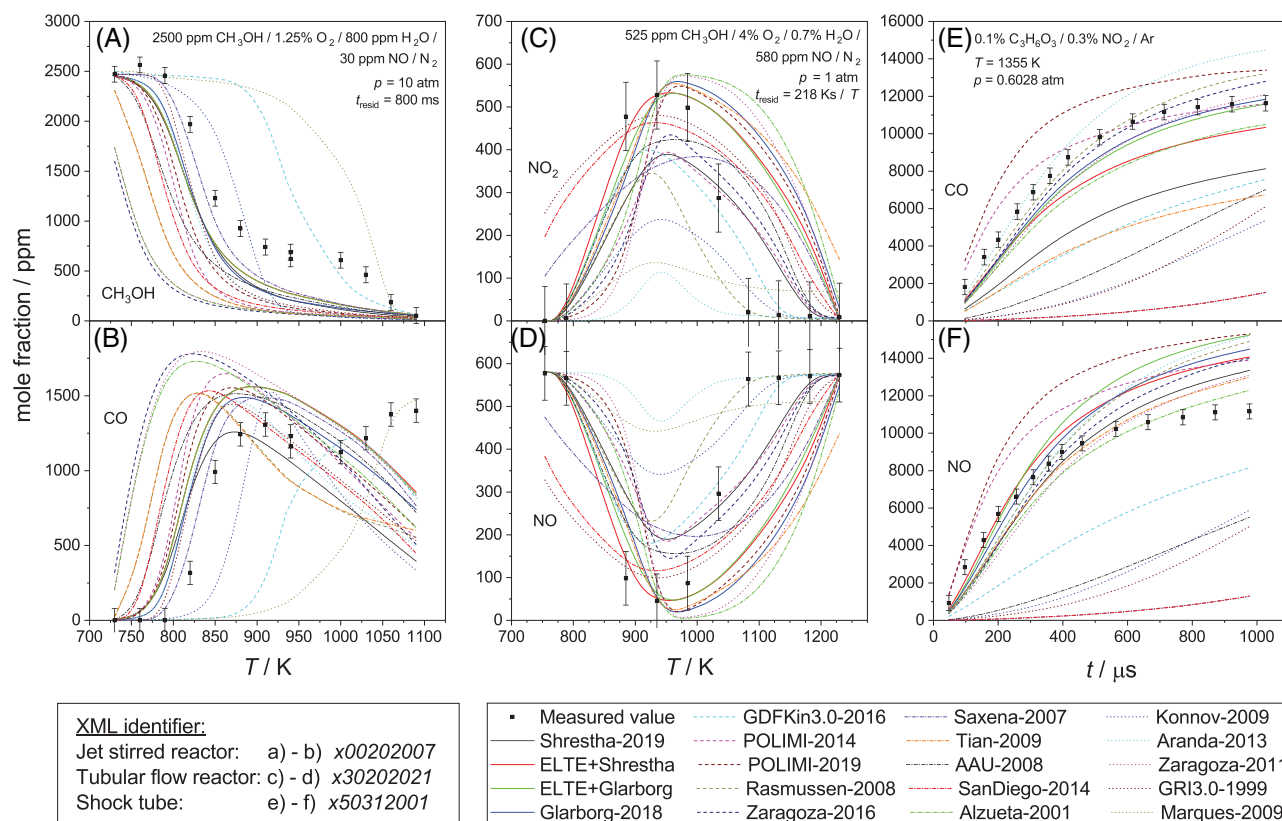
FIGURE 1 Comparison of the experimental values measured in homogenous reactors and the simulation results in the case of some example datasets. (A) and (B) show the simulation of outlet concentrations measured in a jet stirred reactor.[13] (C) and (D) show the simulation of outlet concentrations measured in a tubular flow reactor.[21] (E) and (F) show concentration–time profiles measured in a shock tube.[26] The experimental conditions are shown in the upper figures. Further information can be found in Tables S1–S3 of the Supplementary Material, Part 1 at the given XML identifiers [Color figure can be viewed at wileyonlinelibrary.com]

average, which can be considered as a general requirement for a mechanism.

The obtained simulation results of the 2552 data points, belonging to the 17 mechanisms, were typically very different from each other and sometimes also from the experimental data. For the illustration of the trends and general behavior, some examples are shown for the simulation results of the experiments in homogenous reactors in Figure 1.

For a comprehensive quantitative comparison, error function values E given in Equation (1) were calculated for all datasets and for all mechanisms with three recent combustion simulation solvers, FlameMaster 4.2.1, FlameMaster 4.0.0, and OpenSMOKE++ 0.12.0 (from now on: FM 4.2.1, FM 4.0.0, and OS). We found that the simulation results obtained with the three solvers were in relatively good agreement, but OS had more stable performance in perfectly stirred reactor simulations and it had slightly lower runtimes. The main article contains the only simulation results obtained with OS, and the detailed results obtained with FM are given in the Supplementary Material, Part 1 (see Tables S4 and S5). Table 2 shows the cal-

culated error function values based on the OS simulation results.

The error function value results of a mechanism in Table 2 are grouped in columns based on the different experiment types and also the overall results. The simulation results were filtered according the following criteria: results of a dataset were excluded from the calculation of the E values shown in Table 2 if none of the two best mechanisms (Shrestha-2019 and Glarborg-2018) could reproduce the experiments with $E < 100$. This way 225 datasets, with 2373 data points, were left for comparison. Most of the mechanisms were not able the simulate successfully all datasets due to failed simulations of some data points (except Shrestha-2019, Glarborg-2018, POLIMI-2014, and POLIMI-2019) but the comparison can be done due to the standardization with the scatter of the dataset in the Equation (1) error function value. The final order of the mechanisms is based on the overall (filtered) error function value.

The overall best mechanisms were Shrestha-2019, Glarborg-2018, GDFKin3.0-2016, POLIMI-2014, and POLIMI-2019, respectively, on average with $E < 40$. The

good performance of the GDFKin3.0-2016 mechanism, which was not directly validated to simulate methanol combustion, justifies the reason of the investigation of the mechanisms out of their validation range. The Rasmussen-2008, Zaragoza-2016, Saxena-2007, and Tian-2009 mechanisms have lower but still acceptable performance on simulating NOx perturbed methanol combustion, in average with $E < 50$. The other mechanisms have lower performance (average $E > 50$), which was not unexpected as most of these mechanisms were not validated to simulate methanol combustion in the wide range of experimental conditions.

Despite the failed simulations, Saxena-2007, Glarborg-2018, POLIMI-2019, Shrestha-2019, Aranda-2013, and GDFKin3.0-2016 were the best for JSR simulations, with $E < 30$ on average. Shrestha-2019 was significantly the best for TFR simulations and GDFKin3.0-2016, Glarborg-2018, Zaragoza-2016, POLIMI-2014, and Saxena-2007 had also decent performance with $E < 40$. On ST outlet concentration simulations, the tendencies are slightly different. The best performances had the Zaragoza-2011, Alzueta-2001, Zaragoza-2016, Glarborg-2018, and Rasmussen-2008 mechanisms, respectively, with around $E = 10$. The other mechanisms have significantly worse performance here. However, the ST results have less weight in the overall results, due to the lower number of datasets than those of JSR or TFR. Note, that the different tendencies here are probably due to the different chemistry of these experiments, as $C_3H_6O_3/NO_2$ systems were investigated in these datasets. $C_3H_6O_3$ is 1,3,5-trioxane, which decomposes to three formaldehyde molecules at high temperatures so its combustion can be described with the mechanisms of oxygenated C_1 species.

Two further mechanisms were created and tested in this work. The methanol oxidation submechanism of the best two mechanisms (Shrestha-2019 and Glarborg-2018) was replaced with our previously optimized methanol combustion mechanism developed by Olm et al.,[8] which already includes the reactions of our optimized hydrogen and syngas mechanisms by Varga et Al.[47,48] The rate parameters of nine N/H/O reactions were also updated based on our previous optimization study[49] related to the combustion of hydrogen doped with NOx. These optimization studies were carried out using a large number of experimental and theoretical data related to the specific system, and we may assume that these optimized mechanisms have the best performance on simulating the combustion of these systems. Including these mechanisms as submechanisms into the best literature NOx mechanisms can be considered as extending our optimized methanol mechanism with NOx reactions. These new mechanisms can also be downloaded from the Respecth site.[31] Table 2 shows the error function values belonging to these reac-
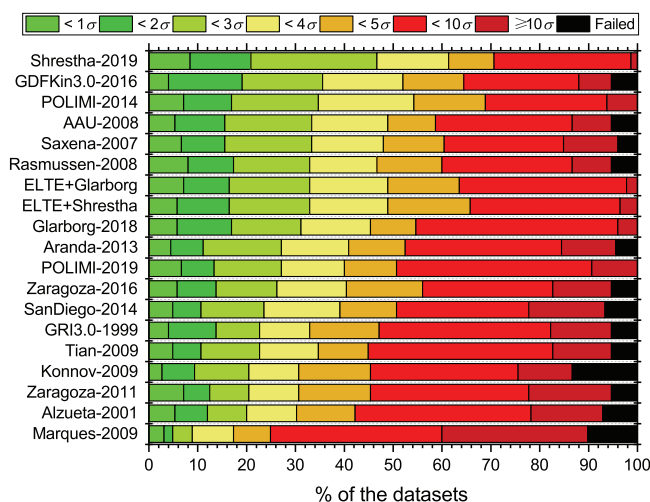

FIGURE 2 Stacked bar plot of the frequencies when the mechanisms could reproduce a dataset within a given threshold of the estimated standard deviation of the dataset. See text for further explanation [Color figure can be viewed at wileyonlinelibrary.com]

tion mechanisms (ELTE+Shrestha and ELTE+Glarborg). The overall performance of these mechanisms is very similar, which may be due to the significant influence of the methanol submechanism. The overall error function values changed from 20.2 to 27.3 and from 31.3 to 27.4 for the Shrestha and Glarborg mechanism pairs, respectively. It means that the replacement of the methanol submechanism and the N/H/O reactions caused decreasing performance in the case of the Shrestha-2019, but improvement in the case of the Glarborg-2018 mechanism. The performance of the mechanisms on the simulation of JSR experiments improved significantly in the case of Shrestha-2019 mechanism (from 27.3 to 21.3) and slightly in the case of the Glarborg-2018 mechanism (from 22.2 to 22.0). In the case of TFR experiments, the performance of the Shrestha-2019 mechanism deteriorated from 16.4 to 31.3 but improved for Glarborg-2018 mechanism from 36.8 to 30.7. The most significant improvement was obtained with the Shrestha-2019 mechanism at the ST outlet concentration simulations (E decreased from 29.7 to 8.5), but at the same time E increased from 10.2 to 14.6 in the case of ST simulations with the Glarborg-2018 mechanism.

Further comparisons of the mechanisms based on OS simulations can be seen in Figures 2 and 3, where the distribution of the error function values is visualized. The corresponding figures obtained with FM can be seen in Figures S1 and S2 of the Supplementary Material, Part 1. Figure 2 shows the frequencies of datasets that were reproduced by the mechanisms within a given threshold of the multiple of the estimated standard deviation. For example, in the case of the Shrestha-2019 mechanism, 46.7% of the datasets were reproduced within 3σ threshold, which
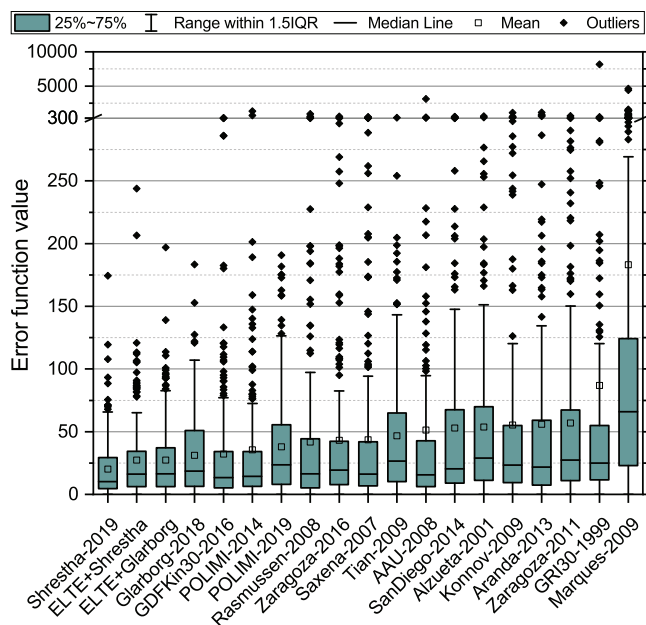
FIGURE 3 Boxes and whiskers plot of the distribution of the error function values of the datasets according to the mechanisms. See text for further explanation [Color figure can be viewed at wileyonlinelibrary.com]

means that 46.7% of the datasets have $E < 9$. The order of the mechanisms in this figure was determined based on this "$<3\sigma$" value with the best mechanism at the top of the figure. It resulted a quite different order compared with Table 2, where the base of the order was the mean error function value. Here, the error function values were not considered, only the count of them within the thresholds. The high values of the outliers can significantly increase the mean error function value resulting in lower ranking in Table 2. Figure 3 shows the boxes and whiskers plot of the error function values of the datasets according to the mechanisms. Here, the order is based on the mean value as well as in Table 2. The median values are also shown, and the boxes correspond to the IQR interquartile range (however, here the first quartile means the best performance) and the whiskers denote the range within 1.5IQR. The outliers are defined here as the values out of 1.5IQR. In this figure, the increase of the mean values due to the outliers is well visible.

Based on these comparisons, Shrestha-2019, Glarborg-2018, and their two modified mechanisms (ELTE+Shrestha, ELTE+Glarborg) were chosen for further investigations using local sensitivity and uncertainty analyses.

4 | LOCAL SENSITIVITY ANALYSIS

Brute force local sensitivity analysis[50,51] was carried out with the four considered mechanisms at the filtered experimental data (2373 data points in 225 datasets). The sensitivity coefficients of the measured concentrations with respect to the A preexponential Arrhenius parameters for each reaction, and also the constant pressure molar heat capacities ($c_{p,j}^{\ominus}(298.15 \text{ K})$), standard enthalpies of formation ($\Delta_f H_j^{\ominus}(298.15 \text{ K})$) and entropies ($S_j^{\ominus}(298.15 \text{ K})$) of each species of these mechanisms were investigated. Langer et al.[52] recently published an article on the investigation of the importance of kinetic and thermodynamic parameters in several nitrogen chemistry combustion systems using local sensitivity and uncertainty analyses.

In the case of the sensitivity analysis of kinetic parameters, the effect of +5% relative perturbation of the A factors was investigated. In the case of the sensitivity analysis of thermodynamic properties, the effect of the absolute perturbation of the corresponding NASA polynomial parameters was investigated. The NASA polynomials describe the temperature dependence of the thermodynamic properties in the mechanisms.[53] For species j, these generalized polynomials are the following:

$$\frac{c_{p,j}^{\ominus}(T)}{R} = a_{1,j} + a_{2,j}T + a_{3,j}T^2 + a_{4,j}T^3 + a_{5,j}T^4 \quad (2)$$

$$\frac{\Delta_f H_j^{\ominus}(T)}{RT} = a_{1,j} + \frac{a_{2,j}}{2}T + \frac{a_{3,j}}{3}T^2$$
$$+ \frac{a_{4,j}}{4}T^3 + \frac{a_{5,j}}{5}T^4 + \frac{a_{6,j}}{T} \quad (3)$$

$$\frac{S_j^{\ominus}(T)}{R} = a_{1,j}\ln T + a_{2,j}T + \frac{a_{3,j}}{2}T^2$$
$$+ \frac{a_{4,j}}{3}T^3 + \frac{a_{5,j}}{4}T^4 + a_{7,j} \quad (4)$$

The $c_{p,j}^{\ominus}$ constant pressure heat capacities were perturbed with an absolute value of +0.08314 J/mol/K via the +0.01 perturbation of $a_{1,j}$. This means a temperature independent shift of the $c_{p,j}^{\ominus}$ values. The perturbation of $a_{1,j}$ affects the calculated enthalpies of formation and entropies, and the perturbation is higher at higher temperatures due to the $a_{1,j}RT$ and $a_{1,j}R\ln T$ terms in the calculation of $\Delta_f H_j^{\ominus}$ and $S_j^{\ominus}$, respectively. The $\Delta_f H_j^{\ominus}$ enthalpies of formation were perturbed with an absolute value of +24.79 J/mol at 298.15 K via the +2.9815 K perturbation of $a_{6,j}$. The $S_j^{\ominus}$ entropies were perturbed with an absolute value of +0.08314 J/mol/K via the +0.01 perturbation of $a_{7,j}$. These perturbations of $\Delta_f H_j^{\ominus}$ and $S_j^{\ominus}$ are temperature independent and the perturbation values were carefully chosen to be within the range of the linear effect.

Table 3 shows the comparison of the most frequently sensitive reactions of the mechanisms. The first 20 reactions with the highest frequencies of significant

TABLE 3 Comparison of the overall sensitivity analysis results of the chemical kinetic parameters (A preexponential factors) of the 20 most sensitive reactions of the four investigated mechanisms

Shrestha-2019			Glarborg-2018			ELTE+Shrestha			ELTE+Glarborg		
Reactions	%	$\lvert sn \rvert_j$	Reactions	%	$\lvert sn \rvert_j$	Reactions	%	$\lvert sn \rvert_j$	Reactions	%	$\lvert sn \rvert_j$
$CH_3OH + OH = CH_2OH + H_2O$	68.0%	0.4252	$CH_3OH + OH = CH_2OH + H_2O$	66.5%	0.3691	$CH_3OH + OH = CH_2OH + H_2O$	68.8%	0.3993	$CH_3OH + OH = CH_2OH + H_2O$	69.5%	0.3909
$H + O_2 + M = HO_2 + M$ (LP)	67.4%	0.3048	$CH_3OH + OH = CH_3O + H_2O$	61.9%	0.3209	$CH_3OH + OH = CH_3O + H_2O$	67.4%	0.3769	$CH_3OH + OH = CH_3O + H_2O$	66.1%	0.3743
$O_2 + H = OH + O$	67.2%	0.3936	$CH_2O + OH = HCO + H_2O$	60.1%	0.2603	$HCO + O_2 = CO + HO_2$	57.6%	0.2792	$HO_2 + OH = H_2O + O_2$	57.9%	0.2850
$CH_3OH + OH = CH_3O + H_2O$	66.0%	0.3729	$H + O_2 = O + OH$	57.8%	0.3042	$HCO + M = H + CO + M$ (LP)	56.8%	0.2680	$H + O_2 = O + OH$	56.4%	0.2950
$CH_2O + OH = HCO + H_2O$	64.7%	0.3045	$HCO + O_2 = CO + HO_2$	56.7%	0.2775	$HO_2 + OH = H_2O + O_2$	56.0%	0.2877	$HCO + O_2 = CO + HO_2$	56.3%	0.2704
$HCO + M = H + CO + M$ (LP)	57.3%	0.2646	$CO + OH = CO_2 + H$	54.0%	0.3313	$H + O_2 = O + OH$	54.2%	0.2825	$HCO + M = H + CO + M$ (LP)	54.6%	0.2555
$NO_2 + H = NO + OH$	56.3%	0.2426	$HCO + M = H + CO + M$	52.0%	0.2348	$NO_2 + H = NO + OH$	53.6%	0.2022	$CO + OH = CO_2 + H$	53.4%	0.3079
$HCO + O_2 = CO + HO_2$	55.2%	0.2649	$H + O_2 + M = HO_2 + M$	48.8%	0.1899	$CO + OH = CO_2 + H$	52.6%	0.3042	$NO_2 + H = NO + OH$	51.6%	0.1951
$CO + OH = CO_2 + H$ (DUP3)	43.6%	0.2215	$NO_2 + H = NO + OH$	48.3%	0.1776	$CH_2O + OH = HCO + H_2O$	50.0%	0.2153	$H + O_2 + M = HO_2 + M$ (LP)	49.6%	0.2027
$CH_2O + OH = HOCH_2O$	43.4%	0.1302	$HO_2 + OH = H_2O + O_2$ (DUP2)	46.1%	0.1916	$H + O_2 + M = HO_2 + M$ (LP)	49.6%	0.2028	$NO + HO_2 = NO_2 + OH$	49.2%	0.2310
$CO + OH = CO_2 + H$ (DUP2)	43.1%	0.1954	$NO + HO_2 = NO_2 + OH$	45.5%	0.2213	$NO + HO_2 = NO_2 + OH$	47.4%	0.2362	$CH_2O + OH = HCO + H_2O$	47.2%	0.2082
$HO_2 + OH = H_2O + O_2$ (DUP1)	42.9%	0.1916	$CH_3OH + NO_2 = HONO + CH_2OH$	40.3%	0.1469	$CH_3OH + NO_2 = HONO + CH_2OH$	37.9%	0.1348	$CH_3OH + NO_2 = HONO + CH_2OH$	37.9%	0.1392
$NO + HO_2 = NO_2 + OH$	38.3%	0.1629	$CH_2O + NO_2 = HONO + HCO$	34.7%	0.1206	$HCO + NO_2 = NO + CO_2 + H$	28.4%	0.1164	$HCO + NO_2 = NO + CO_2 + H$	28.1%	0.1164
$CH_3OH + NO_2 = HONO + CH_2OH$	30.0%	0.1121	$HCO + NO_2 = NO + CO_2 + H$	28.8%	0.1132	$CH_2O + NO_2 = HONO + HCO$	24.4%	0.0977	$NO + OH + M = HONO + M$ (LP)	26.0%	0.1367
$HCO + NO = HNO + CO$	23.5%	0.1016	$HO_2 + OH = H_2O + O_2$ (DUP1)	27.8%	0.0702	$HCO + NO = HNO + CO$	22.8%	0.0907	$CH_2O + NO_2 = HONO + HCO$	20.6%	0.0903
$HCO + NO_2 = NO + CO_2 + H$	22.0%	0.0858	$NO + OH + M = HONO + M$	23.7%	0.1254	$NO + OH + M = HONO + M$ (LP)	18.8%	0.0978	$CH_3OH + O = CH_2OH + OH$	18.3%	0.0482
$NO_2 + O = NO + O_2$	20.8%	0.0712	$HO_2 + HO_2 = H_2O_2 + O_2$ (DUP1)	18.9%	0.0556	$HNO + OH = NO + H_2O$	18.8%	0.0638	$HCO + NO = HNO + CO$	17.4%	0.0689
$CH_2O + NO_2 = HONO + HCO$	18.6%	0.0804	$NO_2 + O = NO + O_2$	18.5%	0.0544	$NO_2 + O = NO + O_2$	17.2%	0.0501	$HONO + OH = NO_2 + H_2O$	16.8%	0.0512
$HNO + OH = NO + H_2O$	18.2%	0.0609	$NO_2 + HO_2 = HNO_2 + O_2$	18.2%	0.0668	$CH_3OH + O = CH_2OH + OH$	15.6%	0.0430	$NO_2 + O = NO + O_2$	16.0%	0.0483
$CH_3OH + O = CH_3O + OH$	18.0%	0.0510	$HCO + NO = HNO + CO$	17.4%	0.0704	$CH_3OH + HO_2 = CH_2OH + H_2O_2$	15.6%	0.0776	$CH_3OH + HO_2 = CH_2OH + H_2O_2$	15.4%	0.0763

LP, low pressure limit reactions; DUP, Duplicate reactions. See text for further explanation.

TABLE 4 Comparison of the overall sensitivity analysis results of the thermodynamic parameters separately for heat capacities, enthalpies of formation, and entropies of the 10 most sensitive species of the four investigated mechanisms

Shrestha-2019			Glarborg-2018			ELTE+Shrestha			ELTE+Glarborg		
Species	%	$\widetilde{\|sn\|}_j$	Species	%	$\widetilde{\|sn\|}_j$	Species	%	$\widetilde{\|sn\|}_j$	Species	%	$\widetilde{\|sn\|}_j$
Heat capacity											
OH	88.4%	0.6168	OH	91.4%	0.6808	OH	94.2%	0.7787	OH	94.2%	0.7687
NO	75.8%	0.4011	NO	83.9%	0.4686	NO	75.7%	0.4289	NO	79.9%	0.4467
HONO	54.2%	0.3751	HONO	62.1%	0.4606	NO_2	51.9%	0.2755	HONO	59.1%	0.4172
$HOCH_2O$	50.7%	0.2962	NO_2	48.8%	0.2895	HONO	49.8%	0.3548	NO_2	42.1%	0.2530
CH_2O	46.8%	0.2137	HO_2	44.7%	0.2382	HO_2	43.7%	0.2475	HO_2	40.9%	0.2198
NO_2	46.7%	0.2321	H_2O	35.9%	0.1484	H_2O_2	31.3%	0.1538	H	31.2%	0.1189
HO_2	43.0%	0.2432	O	32.2%	0.0962	H	31.1%	0.1244	H_2O	30.5%	0.1270
H_2O	36.8%	0.1446	H	29.4%	0.1146	H_2O	31.0%	0.1293	O	27.4%	0.0822
H	33.8%	0.1436	O_2	26.2%	0.0991	O_2	26.0%	0.1049	H_2O_2	26.5%	0.1335
O_2	26.9%	0.1100	N_2	21.5%	0.1063	CH_3ONO	24.1%	0.0655	O_2	25.7%	0.0956
Enthalpy of formation ($\widetilde{\|ssn\|}_j$ instead of $\widetilde{\|sn\|}_j$)											
OH	88.7%	0.7180	OH	91.1%	0.7928	OH	94.6%	0.8449	OH	92.3%	0.8283
NO	78.3%	0.4873	NO	83.5%	0.5624	NO	74.8%	0.4878	NO	78.3%	0.5147
HONO	53.0%	0.3233	HONO	57.3%	0.3867	NO_2	49.1%	0.2492	HONO	52.2%	0.3225
NO_2	48.9%	0.2180	NO_2	48.2%	0.2677	HONO	43.6%	0.2785	NO_2	40.2%	0.2317
CH_2O	47.7%	0.2444	HO_2	45.6%	0.2215	HO_2	43.3%	0.2208	HO_2	39.6%	0.1916
$HOCH_2O$	46.4%	0.2313	O	38.3%	0.1376	H	36.4%	0.1807	H	35.1%	0.1694
HO_2	45.0%	0.2401	H	36.8%	0.1716	O_2	35.6%	0.1327	O	33.6%	0.1189
H_2O	44.1%	0.2028	H_2O	36.6%	0.1589	H_2O	34.0%	0.1203	H_2O	32.5%	0.1120
O_2	42.2%	0.1852	O_2	36.0%	0.1403	CH_3OH	30.9%	0.1053	O_2	31.6%	0.1166
H	40.8%	0.2167	CH_3OH	33.5%	0.1350	O	29.8%	0.1022	H_2O_2	23.6%	0.0937
Entropy											
OH	89.1%	0.6512	OH	90.7%	0.7109	OH	94.2%	0.7902	OH	93.8%	0.7847
NO	77.7%	0.4907	NO	84.7%	0.5520	NO	76.9%	0.4965	NO	80.5%	0.5190
HONO	54.7%	0.3715	HONO	60.1%	0.4484	NO_2	52.8%	0.2829	HONO	57.5%	0.3926
NO_2	50.4%	0.2520	NO_2	51.2%	0.3024	HONO	47.5%	0.3350	NO_2	42.9%	0.2582
$HOCH_2O$	50.1%	0.2871	HO_2	46.5%	0.2595	HO_2	45.0%	0.2554	HO_2	41.2%	0.2263
CH_2O	49.1%	0.2465	O	35.6%	0.1120	H	29.8%	0.1069	O	30.2%	0.0947
HO_2	46.1%	0.2690	H_2O	31.4%	0.1265	H_2O_2	29.4%	0.1339	H	29.4%	0.1028
H	33.7%	0.1368	H	28.3%	0.1050	H_2O	29.0%	0.1104	H_2O	28.8%	0.1094
H_2O	32.3%	0.1267	O_2	26.9%	0.1023	O_2	28.1%	0.1127	O_2	25.5%	0.0993
O_2	32.1%	0.1328	CH_3OH	23.0%	0.0945	O	26.8%	0.0822	H_2O_2	24.7%	0.1147

sensitivities from the four considered mechanisms are shown. Tables S6–S8 of the Supplementary Material, Part 1 show the sensitivity analysis results compared according to experiment type for OS and FM as well. Table 4 provides the comparison of the most frequently sensitive species of the mechanisms. The first 10 species of each thermodynamic property with the highest frequencies of significant sensitivities from the four considered mechanisms are shown. A sensitivity coefficient is considered significant if its normalized absolute value is higher than 10% of the highest absolute normalized sensitivity coefficient

of this data point. The frequency values (the % columns in Tables 3 and 4) show the ratio of these important data points to all data points. The $\widetilde{\|sn\|}_j$ values in Tables 3 and 4 are the mean scaled absolute normalized sensitivity coefficients:

$$\widetilde{\|sn\|}_j = \frac{1}{N_i} \sum_{i=1}^{N_i} \frac{\left|sn_{ij}\right|}{\max \|sn\|_i} \qquad (5)$$

Here, i is the index of the data point and j is the index of the reaction or the thermodynamic parameter of a species

($c^{\ominus}_{p,j}$(298.15 K) or $S^{\ominus}_{j}$(298.15 K)), sn_{ij} is the normalized sensitivity coefficient, which can be calculated in the finite differentiate approximation in the case of relative perturbation as $s\,n_{ij} = (Y'_i - Y_i)/(f_{pert}Y_i)$, where Y_i is the simulation result of data point i, Y'_i is the perturbed value and f_{pert} is the perturbation factor. In the case of absolute perturbation $sn_{ij} = (p_j/d)(Y'_i - Y_i)/Y_i$, where d is the absolute value of perturbation added to parameter p_j. The scaling of the normalized sensitivity coefficients described with Equation (5) were done by dividing with the maximum kinetic, heat capacity, or entropy normalized sensitivity coefficient of a data point in the case of a kinetic, heat capacity, or entropy parameter, respectively. In the case of $\Delta_f H^{\ominus}_j$(298.15 K) enthalpies of formation the normalization described above cannot be implemented as the enthalpies of formation of the different species with different signs and orders of magnitudes would bias the results. For that reason, the semi-normalized sensitivity coefficients of these parameters are investigated with absolute perturbation according to equation $ssn_{ij} = (Y'_i - Y_i)/(d \cdot Y_i)$ and $\widetilde{|ssn|}_j$, the equivalent of $\widetilde{|sn|}_j$ in Equation (5) is calculated with the semi-normalized sensitivity coefficient to identify the parameters with significant sensitivities.

According to Table 3, the sensitivity analysis results of parameters A of the four mechanisms are in good agreement with minor differences. The reactions with the highest frequency of significant sensitivities are the two channels of the $CH_3OH + OH$ reaction with frequencies between 60 and 70% in the case of the Glarborg-2018, ELTE+Shrestha, and ELTE+Glarborg mechanisms. The highest mean scaled normalized sensitivity coefficients belong to these reactions as well with a value around 0.4. In the case of the Shrestha-2019 mechanism, the reactions of $H + O_2$ are also among the most important reactions besides the $CH_3OH + OH$ reactions, but the $H + O_2$ reactions are also important in the cases of the other mechanisms. The next reactions in the list correspond to HCO and CH_2O. The most important nitrogen-containing reaction is the $NO_2 + H = NO + OH$ in the case of each mechanism. The most important (and only) reactions related to the interaction between methanol or formaldehyde and NOx in the table are the following two H-abstraction reactions:

$$CH_3OH + NO_2 = HONO + CH_2OH \qquad (R1)$$

$$CH_2O + NO_2 = HONO + HCO \qquad (R2)$$

The frequency of significant sensitivity of these reactions are within 20–40%, the $\widetilde{|sn|}_j$ values are within 0.08–0.15 for all mechanisms. These reactions can be the subject of fur-

ther investigations as the only reactions with significant sensitivity related specifically to the methanol/NOx system.

The comparison of the sensitivities of different thermodynamic properties is a challenging task, due to their different nature like their definition or unit, that is why their scaling (see Equation (5)) and comparison were done separately in Table 4. Based on this table, the sensitivity analysis results of the thermodynamic properties are also in agreement for the four mechanisms. The species with the most sensitive parameters are OH and NO regardless the thermodynamic property or mechanism, with frequencies between 70 and 95% and $\widetilde{|sn|}_j$ or $\widetilde{|s|}_j$ values around 0.3–0.8. Besides that, HONO and NO_2 usually also have high sensitivities with frequencies around 40–60% and $\widetilde{|sn|}_j$ or $\widetilde{|s|}_j$ values within 0.2–0.4. Further important parameters can be identified based on Table 4, for example, the heat capacity, enthalpy of formation, and entropy of HO_2. Other species, like H, H_2O, O, and O_2, also play a relatively important role in general, as others, like H_2O_2, CH_3OH, or CH_3ONO in some cases. The results of the Shrestha-2019 mechanism are slightly different from the other three mechanisms. Species $HOCH_2O$ and CH_2O appears among the most important species, but the frequencies and $\widetilde{|sn|}_j$ or $\widetilde{|s|}_j$ values of this mechanism are lower than those of the other three mechanisms for the same species.

5 | LOCAL UNCERTAINTY ANALYSIS

Local uncertainty analysis is a suitable method to investigate further the mechanisms of MeOH/NOx combustion. This analysis is a linear estimation of the variances of model results from the variances of the parameters. The main information obtained with this analysis is the origin of uncertainty of the simulated results and the contribution of the uncertainty of the model parameters to it. The method has been discussed in detail by Turányi et al.[51] and Zádor et al.[54] and a brief summary is given here with slightly different notations. If parameters p_j of a model are not correlated, the variance of model output Y_i can be calculated according to the following equations:

$$\sigma^2_{Gj}(Y_i) = \left(\frac{\partial Y_i}{\partial p_j}\right)^2 \sigma^2(p_j) \qquad (6)$$

$$\sigma^2_G(Y_i) = \sum_j \sigma^2_{Gj}(Y_i) \qquad (7)$$

Here, subscript G refers to a group of parameters. This way we can investigate the uncertainty contribution for example the kinetic parameters or a separable group of them like those of the reactions of the nitrogen containing

species, or the uncertainty contribution of thermodynamic species.

In the case of kinetic parameters (G = K), $p_j = \ln A_j$, the logarithm of the A Arrhenius parameter of the j-th reaction, $(\partial Y_i/\partial p_j)^2 = (\partial Y_i/\partial \ln A_j)^2$, the square of the related semi-normalized sensitivity coefficient, and $\sigma^2(p_j) = \sigma^2(\ln A_j)$ the variance of the logarithmic A Arrhenius parameter, which is equal to the variance of the logarithmic rate coefficient $\sigma^2(\ln k_j)$ if the temperature dependence is not taken into account. The $\sigma^2(\ln k_j)$ can be determined based on the following equation[51,55]:

$$\sigma^2\left(\ln k_j\right) = \left(\left(f_j \ln 10\right)/3\right)^2 \qquad (8)$$

Here, f_j is the uncertainty parameter of the j-th reaction defined as:

$$f_j = \log_{10}\left(\frac{k_j^0}{k_j^{\min}}\right) = \log_{10}\left(\frac{k_j^{\max}}{k_j^0}\right) \qquad (9)$$

where k_j^0 is the recommended value of the rate coefficient of reaction j and $k_j^{\min}$ and $k_j^{\max}$ are the extreme values; rate coefficients outside the $[k_j^{\min}, k_j^{\max}]$ interval are considered physically nonrealistic by the evaluators.

In the case of thermodynamic parameters (G = T), the uncertainty contribution of the constant pressure heat capacities was investigated, when $p_j = a_{1,j}$ and $(\partial Y_i/\partial p_j)^2 = (\partial Y_i/\partial a_{1,j})^2$, which is the squared local sensitivity coefficient of the $a_{1,j}$ parameter. In this work, the uncertainty contribution of the standard enthalpies of formation (when $p_j = a_{6,j}$) and the standard entropies (when $p_j = a_{7,j}$) was also considered.

The sum of the variances of the uncorrelated groups of parameters provides the variance of the model results:

$$\sigma^2(Y_i) = \sum_G \sigma_G^2(Y_i) \qquad (10)$$

The $S_G\%_{ij}$ percentage contribution of parameter group G and $S\%_{ij}$ percentage contribution of parameter j to the uncertainty of simulation results can be also calculated, according to Equations (11) and (12), respectively.

$$S_G\%_{ij} = \frac{\sigma_G^2(Y_i)}{\sigma^2(Y_i)} \times 100\% \qquad (11)$$

$$S\%_{ij} = \frac{\sigma_j^2(Y_i)}{\sigma^2(Y_i)} \times 100\% \qquad (12)$$

Local uncertainty analysis of the four considered mechanisms was carried out. Uncertainty parameters f of the reaction steps of the mechanisms were collected mainly from review papers by Baulch et al.,[56–58] Atkinson et al.,[59–61] DeMore et al.,[62] and Tsang et al.[63–66] Also, the uncertainties of some direct experimental and theoretical determinations of the rate coefficients were taken from the NIST Chemical Kinetic Database.[67] In the lack of literature information or when only unreliable data were found, $f_j = 1$ was assumed. This way the uncertainty parameters f of 881 reaction steps of the four mechanisms were collected or estimated wherein 428 uncertainty parameters were assumed to be $f_j = 1$. The uncertainty of the rate coefficient of reaction R1 has not been investigated yet, and the uncertainty factor of reaction R2 was estimated as $f_j = 0.3$ by Tsang et al.,[64] which we considered as too low. Due to the importance of these reactions in the methanol/NOx system, the temperature-dependent uncertainty bands of these reactions were determined. The results of the determination can be seen in Figure S3 of the Supplementary Material, Part 1. A more detailed description of the determination of the prior uncertainty of the rate coefficients of these reactions is available in the *k-evaluation* web page.[68] This interactive website is a database that currently contains the Arrhenius parameters of more than 100 gas phase elementary reactions determined in direct measurements, theoretical calculations or have been used in modeling studies. The users of the website may recalculate the uncertainty limits of the rate coefficients. This way the mean uncertainty parameter value was estimated to be $f_j = 2$ for both reactions R1 and R2 as the temperature dependence was not considered at present in our local uncertainty analysis. These f_j values indicate the rate parameters of these two reactions are really highly uncertain. The ELTE+Shrestha and ELTE+Glarborg mechanisms contain previously optimized hydrogen oxidation, methanol and formaldehyde oxidation, and N/H/O submechanisms, which include the optimized parameters of 47 important reactions. The $f_{\text{posterior}}(T)$ posterior uncertainty parameters of these reactions were also determined during the optimization and the temperature-mean values of them were used here as f_j values, since the temperature dependence of the uncertainty of the rate coefficients was not considered here.

The uncertainty contributions of thermodynamic parameters were also investigated. The $\sigma(\Delta_f H_j^{\ominus}(298.15\ \text{K}))$ values were collected from the ATcT database by Ruscic and Bross.[69] This way the uncertainty of enthalpy of formation of 86 species were collected. In the few cases of missing information in this database (12 species), either the data collection of Sander et al.[70] or the estimated uncertainty based on similar species were applied. The literature data for the $\sigma(S_j^{\ominus}(298.15\ \text{K}))$ uncertainties of gas phase entropies and $\sigma(c_{p,j}^{\ominus}(298.15\ \text{K}))$ uncertainties of heat capacities are much more lacking.

TABLE 5 Comparison of the uncertainty contribution of the thermodynamic and kinetic parameters of the four investigated mechanisms according to experiment types

		$\sigma_K^2(Y_i)$	$\sigma_T^2(Y_i)$	$\sigma^2(Y_i)$	$S_K\%_{ij}$	$S_T\%_{ij}$
JSR	Shrestha-2019	5.20×10^{-5}	1.09×10^{-6}	5.31×10^{-5}	97.9%	2.1%
	Glarborg-2018	5.84×10^{-5}	1.42×10^{-6}	5.98×10^{-5}	97.6%	2.4%
	ELTE+Shrestha	2.23×10^{-5}	9.03×10^{-6}	3.13×10^{-5}	71.2%	28.8%
	ELTE+Glarborg	2.06×10^{-5}	9.32×10^{-6}	3.00×10^{-5}	68.9%	31.1%
TFR	Shrestha-2019	1.33×10^{-3}	3.59×10^{-5}	1.37×10^{-3}	97.4%	2.6%
	Glarborg-2018	1.36×10^{-2}	8.12×10^{-5}	1.37×10^{-2}	99.4%	0.6%
	ELTE+Shrestha	2.56×10^{-4}	1.86×10^{-5}	2.74×10^{-4}	93.2%	6.8%
	ELTE+Glarborg	1.12×10^{-4}	2.05×10^{-5}	1.32×10^{-4}	84.5%	15.5%
ST	Shrestha-2019	8.33×10^{-4}	3.41×10^{-5}	8.67×10^{-4}	96.1%	3.9%
	Glarborg-2018	8.70×10^{-4}	4.18×10^{-5}	9.12×10^{-4}	95.4%	4.6%
	ELTE+Shrestha	9.35×10^{-4}	3.46×10^{-5}	9.70×10^{-4}	96.4%	3.6%
	ELTE+Glarborg	8.91×10^{-4}	5.03×10^{-5}	9.41×10^{-4}	94.7%	5.3%
Overall	Shrestha-2019	2.22×10^{-3}	7.11×10^{-5}	2.29×10^{-3}	96.9%	3.1%
	Glarborg-2018	1.46×10^{-2}	1.24×10^{-4}	1.47×10^{-2}	99.2%	0.8%
	ELTE+Shrestha	1.21×10^{-3}	6.21×10^{-5}	1.28×10^{-3}	95.1%	4.9%
	ELTE+Glarborg	1.02×10^{-3}	8.01×10^{-5}	1.10×10^{-3}	92.7%	7.3%

σ^2 values show the absolute variances of the corresponding parameter group, whereas S% values show the percentage contribution of them to the overall uncertainty of the experiment type by the given mechanism. (subscripts: K, kinetic contribution; T: thermodynamic contribution; none: overall values).

The uncertainty of entropy of 30 key species were obtained from or estimated based on the data collections by Cox et al.,[71] Chase,[72] and Sander et al.[70] The NASA polynomials of the 17 investigated mechanisms were used to determine uncertainty to the other 56 species without specified uncertainty of entropy and to the heat capacity of all the 86 species. The temperature functions of these properties of these species were calculated based on the polynomials and the mean difference in the temperature range of 1500–2000 K of the recommended (usually the Glarborg-2018 or the mean value in lack of data) and the most extreme function (excluding outliers) was assigned to be the uncertainty of the given property of the given species. This way 258 uncertainties were collected or estimated assigned to heat capacities, enthalpies of formation, and entropies. Then they were divided by R as the effect of the $a_{1,j}$, $a_{6,j}$, and $a_{7,j}$ parameters was investigated. More details about it and all the collected and estimated uncertainties of the thermodynamic and kinetic parameters can be found in the Supplementary Material, Part 2.

Table 5 shows the comparison of the uncertainty contribution of the thermodynamic and kinetic parameters of the four investigated mechanisms according to experiment types. Table 5 also shows the percentage ratio of the uncertainty contribution of these parameter groups to the $\sigma^2(Y_i)$ overall uncertainty of the mechanisms, which is the sum of all the calculated uncertainties of the simulation results with the given mechanism according to Equations (6), (7), and (10).

Based on Table 5, the highest uncertainty belongs to the Glarborg-2018 mechanism with $\sigma^2(Y_i) = 1.47 \times 10^{-2}$, and the Shrestha-2019 and ELTE+Shrestha mechanisms have lower overall uncertainties by an order of magnitude with $\sigma^2(Y_i) = 2.29 \times 10^{-3}$ and 1.28×10^{-3}, respectively. The overall uncertainty of the ELTE+Glarborg mechanism is the lowest with the value of $\sigma^2(Y_i) = 1.10 \times 10^{-3}$. The main contribution of the overall uncertainty is due to the kinetic parameters to the TFR simulation results in the case of Glarborg-2018 and Shrestha-2019, but in the case ELTE+Shrestha and ELTE+Glarborg mechanism, the highest contribution is due to the kinetic uncertainty of ST simulations. The thermodynamic parameters have significant overall uncertainty contributions in some cases, especially for JSR simulations with the ELTE-modified mechanisms where posterior uncertainties obtained from optimization were used for some kinetic parameters. These posterior uncertainties were much lower than the prior ones used in the uncertainty analyses of the Shrestha-2019 and Glarborg-2018 mechanisms.

More valuable information could be obtained via investigating not only the overall uncertainties, but also the contribution to the uncertainty of a specific group of simulation results. Note, that all the Y_i model outputs are from the simulations of concentration profiles expressed in mole fractions, so all the $\sigma^2(Y_i)$ values are unitless. Usually, the order of magnitude of the measured concentrations of different species can vary widely, and so the variances, therefore the comparison of the absolute values of the variances

is not sufficient. More information could be obtained via the investigation of the percentage uncertainty contribution of a group of parameters to a group of simulation results. For example, the uncertainty contribution of the parameters of nitrogen containing reactions to the simulation of NO outlet concentrations in JSRs can be investigated. Figure 4 shows the results of this type for the interpretation of the local uncertainty analysis results of the four mechanisms.

The distributions of uncertainty contribution between parameter groups are in a relatively good agreement for the mechanisms except for in a few cases. In general, the main part of the uncertainty of the simulation results is due to the uncertainty of nitrogen chemistry. However, the CO and CO_2 profiles in JSRs, and the CO profiles in TFRs have significant uncertainties due to the parameters of H_2/O_2 and syngas reactions, especially in the case of Shrestha-2019 and Glarborg-2018 mechanisms. In these mechanisms, the parameters of hydrogen oxidation and C_1 chemistry as the oxidation of methanol and formaldehyde dominate the uncertainty of H_2O, CH_2O, and CH_3OH profiles in JSRs and (next to the nitrogen chemistry) the uncertainty of CH_2O, NO, and NO_2 profiles in TFRs. The uncertainty in ST simulations is mainly from the nitrogen chemistry. The overall effect of the thermodynamic contribution is not significant; however, it is unexpectedly important in some cases. The main origin of the thermodynamic uncertainty is parameter $a_{1,j}$, which means the uncertainty of the heat capacity, but which also causes a high uncertainty of the calculated enthalpies of formation and entropies at high temperatures. The room temperature uncertainties of enthalpies of formation and entropies (parameters $a_{6,j}$ and $a_{7,j}$), which cause temperature independent shifts of these values are relatively small and their effect can be barely seen in the figure. Note, that this is due to the chemical kinetics of the investigated system and the uncertainties of these parameters may cause large uncertainty of the simulation results in other chemical systems, like the low temperature oxidation of hydrocarbons.[73] Calculated concentrations of several species have been influenced remarkably by the thermodynamic parameters mainly in JSR simulations with the ELTE modified mechanisms, but COx and NOx species have been affected in TFRs as well with all mechanisms. But the uncertainty of other species in TFRs and STs also has considerable thermodynamic effect. The largest of such effects have been obtained for CH_2O profile in JSRs with ELTE+Shrestha mechanism. About 80% of the uncertainty of these simulation results have of thermodynamic origin. The second largest thermodynamic effect, about 60%, was obtained for CO_2 profile in TFRs with Shrestha-2019 mechanism. The effect of using posterior uncertainties is clearly visible at all the JSR and the overall TFR data, where the thermodynamic contribu-
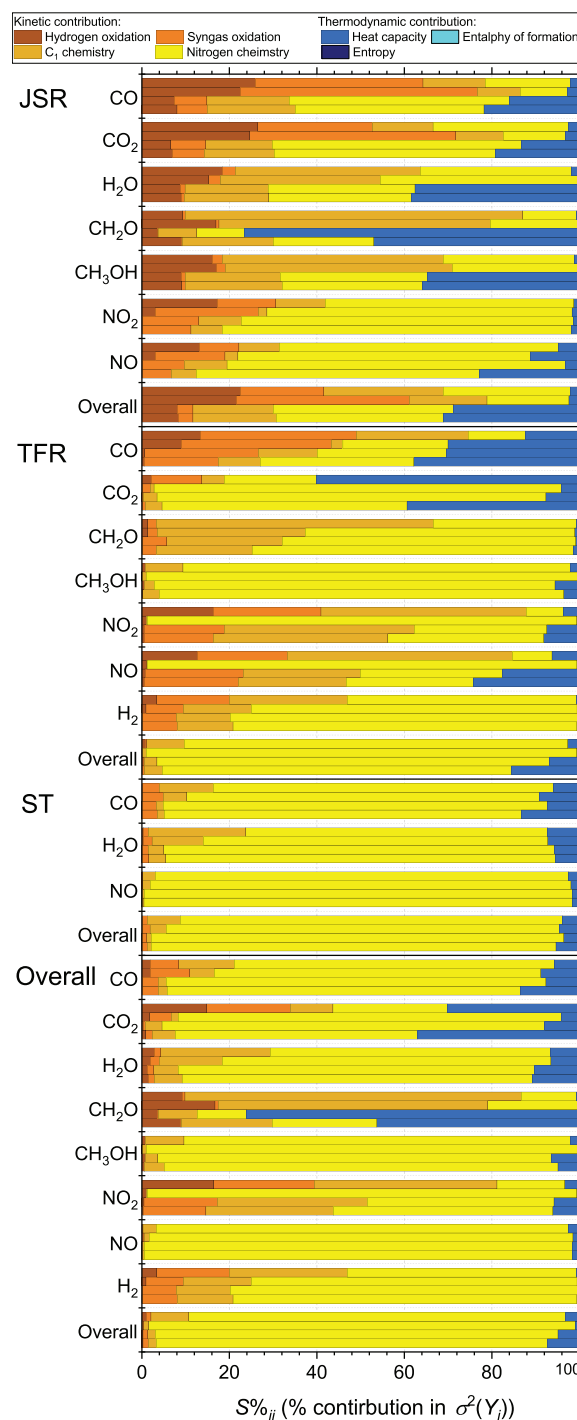
FIGURE 4 The percentage contribution of the uncertainty of a parameter group to the uncertainty of a specific group of simulation results. The effects of parameter groups defined in the label at the top of the figure were investigated. The grouped simulation results are the outlet concentrations in mole fraction of the given species from the given reactor according to the y-axis. The overall values for a reactor (at the bottom of the panel of the reactor) and for a species (in the bottom panel) are also shown. The four bars within a bar-group of a species correspond to the mechanisms from top to bottom in the following order: Shrestha-2019, Glarborg-2018, ELTE+Shrestha, and ELTE+Glarborg [Color figure can be viewed at wileyonlinelibrary.com]
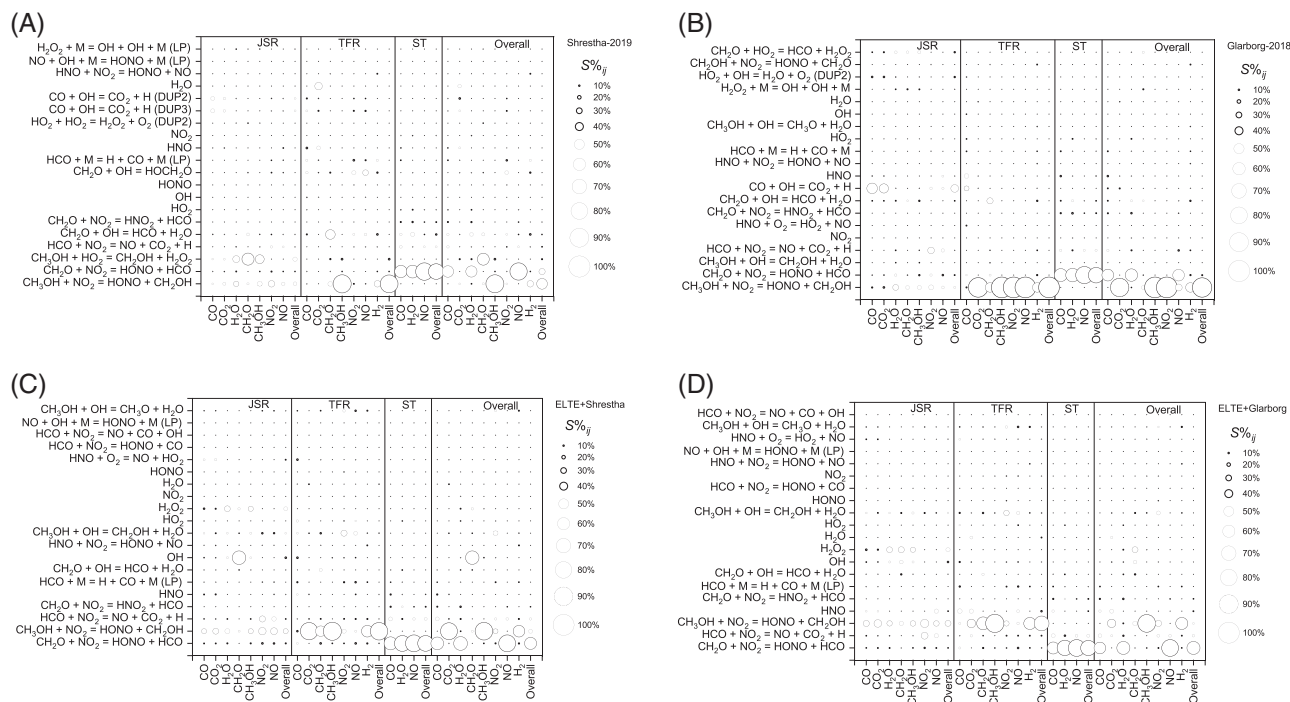
FIGURE 5 Parameters with the largest uncertainty contributions of the (A) Shrestha-2019, (B) Glarborg-2018, (C) ELTE+Shrestha, and (D) ELTE+Glarborg mechanisms. The uncertainty contributions of the ln k_j value of the reactions or the heat capacity of the species in the y-axis to the simulated value of a given species in x-axis in a reactor named at the top of the corresponding panels was investigated. The size of the circles in the corresponding intersection shows the percentage contribution according to the scale in the right-hand side of the figures. The overall values for a reactor and for a species are also shown

tion of the ELTE+Glarborg and ELTE+Shrestha mechanisms is larger than for the original mechanisms due to the lower f_j values of 60 optimized kinetic parameters.

The origin of the uncertainties can be determined in an even more detailed way by considering the contributions of individual parameters to the group of model outputs. Figure 5 shows the more detailed results of the local uncertainty analysis via the parameters with largest uncertainty contribution of the (A) Shrestha-2019, (B) Glarborg-2018, (C) ELTE+Shrestha, and (D) ELTE+Glarborg mechanisms. The figures show the first 20 reactions and species in the order based on the overall uncertainty contribution of their investigated property (ln k_j or $c_{p,j}^{\ominus}$).

As it can be clearly seen on Figure 5, the reactions with the highest uncertainty contribution are:

$$CH_3OH + NO_2 = HONO + CH_2OH \quad (R1)$$

$$CH_2O + NO_2 = HONO + HCO \quad (R2)$$

The uncertainty of R1 causes the 50.5%, 91.1%, 18.5%, and 9.2%, whereas the uncertainty of R2 causes the 29.5%, 5.0%, 57.6%, and 62.03% of the overall uncertainty of Shrestha-2019, Glarborg-2018, ELTE+Shrestha, and ELTE+Glarborg mechanisms, respectively. R1 is the

most significant for the TFR and JSR, whereas R2 is the most significant in the ST measurements. The JSR and TFR measurements correspond to methanol experiments, whereas the ST measurements correspond to formaldehyde experiments. The overall picture is similar in the cases of the four mechanisms, and there are only slight differences regarding the order of the parameters. Some of the further reactions with high uncertainty contribution for all the mechanisms are $HCO + NO_2 = NO + CO_2 + H$, $CH_2O + NO_2 = HNO_2 + HCO$, and $CH_3OH + OH = CH_2OH + H_2O$. The thermodynamic properties with the highest uncertainty contributions are the heat capacity of HNO, OH, HO_2, and NO_2, as these species appear most frequently in Figure 5 with significant contribution values, and those of H_2O_2, H_2O, and HONO can also be mentioned.

6 | CONCLUSIONS

A comprehensive comparison of 17 recent reaction mechanisms describing the interaction of methanol and formaldehyde with nitrogen oxides in combustion systems was carried out based on large number of experimental data collected from literature. This collection consists of 2552 data points in 243 datasets related to concentration

profile measurements in JSRs, TFRs, and STs. Simulation of these data were carried out with FlameMaster 4.0.0, FlameMaster 4.2.1 and OpenSMOKE++ 0.12.0. The results obtained with OpenSMOKE++ are presented in the main text due to the slightly more stable performance of this solver for JSR simulations, and the results obtained with FlameMasters are given in the Supplementary Material, Part 1. Based on this comprehensive comparison, the Shrestha-2019 and Glarborg-2018 mechanisms have the best performance on the simulation of CH_3OH/NOx and CH_2O/NOx experiments, whereas the GDFKin3.0-2018, POLIMI-2014, and POLIMI-2019 mechanisms have acceptable performance. The other mechanisms have moderate or poor performance, although not all the investigated mechanisms were created for or validated to simulate methanol combustion. Note, that the overall error function value of the Shrestha-2019 mechanism is around $E = 20$, which means even the best mechanism can reproduce the experimental datasets only beyond the 4σ boundaries ($E = 16$) on average. This fact indicates the necessity of further investigations and development of mechanisms for this chemical system.

The two best mechanisms (Shrestha-2019 and Glarborg-2018) and the modified versions of them (ELTE+Shrestha and ELTE+Glarborg) were chosen for further analyses. The modified versions were created with the replacement of the hydrogen, syngas, and methanol oxidation submechanisms and the parameters of nine N/H/O reactions of the original mechanisms to the optimized ones from our previous studies. The local sensitivity analysis of these four mechanisms was carried out and comparison of the results were provided. In the case of each mechanism, the most important reactions related to the interaction of C_1 species and NOx were the $CH_3OH + NO_2 = HONO + CH_2OH$ (R1) and the $CH_2O + NO_2 = HONO + HCO$ (R2) hydrogen-abstraction reactions. The sensitivity of thermodynamic parameters was also considered and the sensitivity of the thermodynamic properties of species OH, NO, HONO, and NO_2 were found to be significant.

Local uncertainty analysis of these mechanisms was also carried out for identifying the uncertainty contributions of the kinetic and thermodynamic parameters of the mechanisms to the uncertainty of the simulation results. To perform this analysis, large number of kinetic and thermodynamic uncertainty parameters was collected from the literature or estimated, which are summarized in the Supplementary Material, Part 2. The largest uncertainty contributions were usually assigned to the parameters of nitrogen containing reactions. The highest contribution belonged to reactions R1 and R2 in the case of each mechanism. For example, in the case of Glarborg-2018 mechanism, 91.1% of the overall uncertainty is caused by R1. Some further reactions, like $HCO + NO_2 = NO +$ $CO_2 + H$, $CH_2O + NO_2 = HNO_2 + HCO$, and $CH_3OH + OH = CH_2OH + H_2O$ have also significant uncertainty contribution in the cases of all mechanisms. Based on the uncertainty analysis results, reactions R1 and R2 require further investigations. The reduction of their uncertainties could be efficient to reduce the overall uncertainties related to the simulation of MeOH/NOx systems. The usage of optimized parameters with low posterior uncertainties effectively decreased the uncertainty contribution of kinetic parameters. One may also take into account the uncertainty contribution of thermodynamic properties such as molar heat capacity, standard molar enthalpy of formation, and standard molar entropy of the species of the mechanisms. Uncertainty of the heat capacity of species HNO, OH, HO_2, and NO_2 has remarkable contribution to the uncertainty of the simulated concentrations of species NO, NO_2, CO, and CO_2 in JSRs and TFRs. This finding is in agreement with that of Langer et al.[52] who found that the simulated NO formation in methane/air flames and the calculated laminar burning velocity of ammonia/air flames can be significantly improved by using better heat capacity values. The heat capacity of some other species also has significant uncertainty contribution in some cases, but the temperature-independent uncertainty of enthalpies of formation and entropies was found to be negligible in the investigated systems compared with those of the heat capacities. However, the literature information is very limited about the uncertainties of heat capacities and entropies.

DATA AVAILABILITY STATEMENT

The data that support the findings of this study are openly available in the ReSpecTh information system at http://respecth.chem.elte.hu/respecth/reac/experiment.php, MeOH/NOx tab.

ORCID

Márton Kovács https://orcid.org/0000-0003-3110-2934
Máté Papp https://orcid.org/0000-0001-5143-6646
István Gy. Zsély https://orcid.org/0000-0002-6512-670X
Tamás Turányi https://orcid.org/0000-0002-1461-165X

REFERENCES

1. Miller D, Frenklach M. Sensitivity analysis and parameter estimation in dynamic modeling of chemical kinetics. *Int J Chem Kinet.* 1983;15(7):677-696. https://doi.org/10.1002/kin.550150709.

2. Frenklach M. Transforming data into knowledge-Process Informatics for combustion chemistry. *Proc Combust Inst*. 2007;31 I(1):125-140. https://doi.org/10.1016/j.proci.2006.08.121.

3. Sheen DA, Wang H. The method of uncertainty quantification and minimization using polynomial chaos expansions. *Combust Flame*. 2011;158(12):2358-2374. https://doi.org/10.1016/j.combustflame.2011.05.010.

4. Wang H, Sheen DA. Combustion kinetic model uncertainty quantification, propagation and minimization. *Prog Energy Combust Sci*. 2015;47:1-31. https://doi.org/10.1016/j.pecs.2014.10.002.

5. Cai L, Pitsch H. Mechanism optimization based on reaction rate rules. *Combust Flame*. 2014;161(2):405-415. https://doi.org/10.1016/j.combustflame.2013.08.024.

6. Cai L, Pitsch H, Mohamed SY, et al. Optimized reaction mechanism rate rules for ignition of normal alkanes. *Combust Flame*. 2016;173:468-482. https://doi.org/10.1016/j.combustflame.2016.04.022.

7. Turányi T, Nagy T, Zsély IG, et al. Determination of rate parameters based on both direct and indirect measurements. *Int J Chem Kinet*. 2012;44(5):284-302. https://doi.org/10.1002/kin.20717.

8. Olm C, Varga T, Valkó É, Curran HJ, Turányi T. Uncertainty quantification of a newly optimized methanol and formaldehyde combustion mechanism. *Combust Flame*. 2017;186:45-64. https://doi.org/10.1016/j.combustflame.2017.07.029.

9. Pitsch H, FlameMaster v4.2.1: A C++ Computer Program for 0D Combustion and 1D Laminar Flame Calculations. Published 2020. https://www.itv.rwth-aachen.de/downloads/flamemaster

10. Pitsch H, FlameMaster v4.0.0: A C++ Computer Program for 0D Combustion and 1D Laminar Flame Calculations. Published 2018. https://www.itv.rwth-aachen.de/downloads/flamemaster

11. Cuoci A, Frassoldati A, Faravelli T, Ranzi E. OpenSMOKE++: an object-oriented framework for the numerical modeling of reactive systems with detailed kinetic mechanisms. *Comput Phys Commun*. 2015;192:237-264. https://doi.org/10.1016/j.cpc.2015.02.014.

12. Cuoci A, Frassoldati A, Faravelli T, Ranzi E, OpenSMOKE++ 0.12.0. Published 2020. https://www.opensmokepp.polimi.it/

13. Dayma G, Ali KH, Dagaut P. Experimental and detailed kinetic modeling study of the high pressure oxidation of methanol sensitized by nitric oxide and nitrogen dioxide. *Proc Combust Inst*. 2007(1):411-418. https://doi.org/10.1016/j.proci.2006.07.143.

14. Moréac G, Dagaut P, Roesler JF, Cathonnet M. Nitric oxide interactions with hydrocarbon oxidation in a jet-stirred reactor at 10 atm. *Combust Flame*. 2006;145(3):512-520. https://doi.org/10.1016/j.combustflame.2006.01.002.

15. Singh S, Grosshandler W, Malte PC, Crain RW. Oxides of nitrogen formed in high-intensity methanol combustion. *Symp Combust*. 1979;17(1):689-699. https://doi.org/10.1016/S0082-0784(79)80068-5.

16. Rasmussen CL, Wassard KH, Dam-Johansen K, Glarborg P. Methanol oxidation in a flow reactor: implications for the branching ratio of the CH3OH+OH reaction. *Int J Chem Kinet*. 2008;40(7):423-441. https://doi.org/10.1002/kin.20323.

17. Xiao C-X, Yan N, Zou M, et al. NO2-catalyzed deep oxidation of methanol: experimental and theoretical studies. *J Mol Catal A Chem*. 2006;252(1):202-211. https://doi.org/10.1016/j.molcata.2006.02.064.

18. Jazbec M, Haynes B, Kinetic Study of Methanol Oxidation and the Effect of NOX at Low Oxygen Concentrations. *5th Asia-Pacific Conf Combust ASPACC 2005 Celebr Prof Bob Bilger's 70th Birthd*. Published online January 1, 2005.

19. Alzueta MU, Bilbao R, Finestra M. Methanol oxidation and its interaction with nitric oxide. *Energy Fuels*. 2001;15(3):724-729. https://doi.org/10.1021/ef0002602.

20. Taylor PH, Cheng L, Dellinger B. The influence of nitric oxide on the oxidation of methanol and ethanol. *Combust Flame*. 1998;115(4):561-567. https://doi.org/10.1016/S0010-2180(98)00028-5.

21. Hjuler K, Glarborg P, Dam-Johansen K. Mutually promoted thermal oxidation of nitric oxide and organic compounds. *Ind Eng Chem Res*. 1995;34(5):1882-1888. https://doi.org/10.1021/ie00044a040.

22. Hjuler K, Dam-Johansen K. Simultaneous NOx–SOx removal by ammonia using methanol injection and partial flue gas condensation. *Environ Prog*. 1993;12(4):300-305. https://doi.org/10.1002/ep.670120411.

23. Lyon RK, Cole JA, Kramlich JC, Chen SL. The selective reduction of SO3 to SO2 and the oxidation of NO to NO2 by methanol. *Combust Flame*. 1990;81(1):30-39. https://doi.org/10.1016/0010-2180(90)90067-2.

24. Murakami N, Kojima N, Hashiguchi M. Oxidation of NO to NO2 in the Flue Gas (I). *J Fuel Soc Japan*. 1982;61(4):276-284. https://doi.org/10.3775/jie.61.276.

25. Glarborg P, Alzueta MU, Kjærgaard K, Dam-Johansen K. Oxidation of formaldehyde and its interaction with nitric oxide in a flow reactor. *Combust Flame*. 2003;132(4):629-638. https://doi.org/10.1016/S0010-2180(02)00535-7.

26. Lin C-Y, Wang H-T, Lin MC, Melius CF. A shock tube study of the CH2O + NO2 reaction at high temperatures. *Int J Chem Kinet*. 1990;22(5):455-482. https://doi.org/10.1002/kin.550220504.

27. Varga T, Olm C, Papp M, Busai Á, Zsély IG, ReSpecTh Kinetics Data Format Specification v2.3. Published online 2020. http://respecth.chem.elte.hu/respecth/reac/ReSpecTh_Kinetics_Data_Format_Specification_v2.3.pdf

28. Frenklach M, PrIMe Webpage. http://www.primekinetics.org/

29. Varga T, Papp M, Busai Á, Zsély IG, Optima++ Package v2.0.0: A General C++ Framework for Performing Combustion Simulations and Mechanism Optimization. Published online 2020. http://respecth.hu

30. Nagy T, Minimal Spline Fit: Introducing Root-Mean-Square Fitting of Data Series with Akima Splines. http://respecth.hu

31. ELTE Chemical Kinetics Laboratory and MTA-ELTE Complex Chemical Systems Research Group, ELTE Institute of Chemistry. ReSpecTh webpage. Accessed August 31, 2020. http://www.respecth.hu

32. Shrestha KP, Seidel L, Zeuch T, Mauss F. Kinetic modeling of NOx formation and consumption during methanol and ethanol oxidation. *Combust Sci Technol*. 2019;191(9):1628-1660. https://doi.org/10.1080/00102202.2019.1606804.

33. Glarborg P, Miller JA, Ruscic B, Klippenstein SJ. Modeling nitrogen chemistry in combustion. *Prog Energy Combust Sci*. 2018;67:31-68. https://doi.org/10.1016/j.pecs.2018.01.002.

34. Lamoureux N, Merhubi HEl, Pillier L, de Persis S, Desgroux P. Modeling of NO formation in low pressure premixed

flames. *Combust Flame*. 2016;163:557-575. https://doi.org/10.1016/j.combustflame.2015.11.007.

35. The CRECK Modeling Group. C1-C3 mechanism (Version 1412, December 2014). Published 2014. Accessed June 11, 2019. http://creckmodeling.chem.polimi.it/

36. Song Y, Marrodán L, Vin N, et al. The sensitizing effects of NO_2 and NO on methane low temperature oxidation in a jet stirred reactor. *Proc Combust Inst*. 2019;37(1):667-675. https://doi.org/10.1016/j.proci.2018.06.115.

37. Alzueta MU, Zaragoza-2016 Mechanism (October 2016) personal communication. Published online 2016.

38. Saxena P, Williams FA. Numerical and experimental studies of ethanol flames. *Proc Combust Inst*. 2007;31:1149-1156. https://doi.org/10.1016/j.proci.2006.08.097.

39. Tian Z, Li Y, Zhang L, Glarborg P, Qi F. An experimental and kinetic modeling study of premixed NH_3 /CH_4 /O_2 /Ar flames at low pressure. *Combust Flame*. 2009;156(7):1413-1426. https://doi.org/10.1016/j.combustflame.2009.03.005.

40. Zabetta EC, Hupa MMM, Coda Zabetta E, Hupa MMM. A detailed kinetic mechanism including methanol and nitrogen pollutants relevant to the gas-phase combustion and pyrolysis of biomass-derived fuels. *Combust Flame*. 2008;152(1-2):14-27. https://doi.org/10.1016/j.combustflame.2007.06.022.

41. Mechanical and Aerospace Engineering (Combustion Research) University of California at San Diego. San Diego Mechanism, version 2014-10-04. Published 2014. Accessed February 18, 2021. http://web.eng.ucsd.edu/mae/groups/combustion/mechanism.html

42. Konnov AA. Implementation of the NCN pathway of prompt-NO formation in the detailed reaction mechanism. *Combust Flame*. 2009;156(11):2093-2105. https://doi.org/10.1016/j.combustflame.2009.03.016.

43. Aranda V, Christensen JM, Alzueta MU, et al. Experimental and kinetic modeling study of methanol ignition and oxidation at high pressure. *Int J Chem Kinet*. 2013;45(5):283-294. https://doi.org/10.1002/kin.20764.

44. Esarte C, Peg M, Ruiz MP, Millera Á, Bilbao R, Alzueta MU. Pyrolysis of ethanol: gas and soot products formed. *Ind Eng Chem Res*. 2011;50(8):4412-4419. https://doi.org/10.1021/ie1022628.

45. Smith GP, Golden DM, Frenklach M, et al. GRI-Mech 3.0. Published 1999. Accessed February 18, 2021. http://combustion.berkeley.edu/gri-mech/index.html

46. Marques CST, dos Santos LR, Sbampato ME, Barreta LG, dos Santos AM. Temperature measurements by OH-LIF and chemiluminescence kinetic modeling for ethanol flames. *Quim Nova*. 2009;32(8):2073-2077. https://doi.org/10.1590/s0100-40422009000800017.

47. Varga T, Nagy T, Olm C, et al. Optimization of a hydrogen combustion mechanism using both direct and indirect measurements. *Proc Combust Inst*. 2015;35(1):589-596. https://doi.org/10.1016/j.proci.2014.06.071.

48. Varga T, Olm C, Nagy T, et al. Development of a joint hydrogen and syngas combustion mechanism based on an optimization approach. *Int J Chem Kinet*. 2016;48:407-422. https://doi.org/10.1002/kin.21006.

49. Kovács M, Papp M, Zsély IG, Turányi T. Determination of rate parameters of key N/H/O elementary reactions based on H_2/O_2/NOx combustion experiments. *Fuel*. 2020;264:116720. https://doi.org/10.1016/J.FUEL.2019.116720.

50. Turányi T, Tomlin AS. *Analysis of Kinetic Reaction Mechanisms*. Springer; 2014. https://doi.org/10.1007/978-3-662-44562-4.

51. Turányi T, Zalotai L, Dóbé S, Bérces T. Effect of the uncertainty of kinetic and thermodynamic data on methane flame simulation results. *Phys Chem Chem Phys*. 2002;4(12):2568-2578. https://doi.org/10.1039/b109154a.

52. Langer R, Lotz J, Cai L, et al. Adjoint sensitivity analysis of kinetic, thermochemical, and transport data of nitrogen and ammonia chemistry. *Proc Combust Inst*. 2021;38. https://doi.org/10.1016/j.proci.2020.07.020.

53. McBride B, Gordon S, Reno M. Coefficients for calculating thermodynamic and transport properties of individual species. *NASA Techical Memomorandum*. 1993;4513(NASA-TM-4513):98. https://ntrs.nasa.gov/citations/19940013151.

54. Zádor J, Zsély IG, Turányi T, Ratto M, Tarantola S, Saltelli A. Local and global uncertainty analyses of a methane flame model. *J Phys Chem A*. 2005;109(43):9795-9807. https://doi.org/10.1021/jp053270i.

55. Turányi T. Sensitivity analysis of complex kinetic systems. tools and applications. *J Math Chem*. 1990;5:203-248.

56. Baulch DL, Bowman CT, Cobos CJ, et al. Evaluated kinetic data for combustion modeling: supplement II. *J Phys Chem Ref Data*. 2005;34(3):757-1397. https://doi.org/10.1063/1.1748524.

57. Baulch DL, Cobos CJ, Cox RA, et al. Evaluated kinetic data for combustion modeling. Supplement I. *J Phys Chem Ref Data*. 1994;23(6):847-848. https://doi.org/10.1063/1.555953.

58. Baulch DL, Cobos CJ, Cox RA, et al. Evaluated kinetic data for combustion modelling. *J Phys Chem Ref Data*. 1992;21(3):411-734. https://doi.org/10.1063/1.555908.

59. Atkinson R, Baulch DL, Cox RA, et al. Evaluated kinetic and photochemical data for atmospheric chemistry: volume I – gas phase reactions of Ox, HOx, NOx and SOx species. *Atmos Chem Phys*. 2004;4(6):1461-1738. https://doi.org/10.5194/acp-4-1461-2004.

60. Atkinson R, Baulch DL, Cox RA, et al. Evaluated kinetic, photochemical and heterogeneous data for atmospheric chemistry: supplement V. IUPAC subcommittee on gas kinetic data evaluation for atmospheric chemistry. *J Phys Chem Ref Data*. 1997;26(3):521-1011. https://doi.org/10.1063/1.556011.

61. Atkinson R, Baulch DL, Cox RA, Hampson RF, Kerr (Chairman) JA, Troe J. Evaluated kinetic and photochemical data for atmospheric chemistry: supplement III. IUPAC subcommittee on gas kinetic data evaluation for atmospheric chemistry. *J Phys Chem Ref Data*. 1989;18(2):881-1097. https://doi.org/10.1063/1.555832.

62. DeMore WB, Golden DM, Hampson RFJ, et al. Chemical Kinetics and Photochemical Data for Use in Stratospheric Modeling, Evaluation Number 11, JPL Publication 94-26. Published online 1994. https://jpldataeval.jpl.nasa.gov/

63. Tsang W. Chemical kinetic data base for propellant combustion. II. Reactions involving CN, NCO, and HNCO. *J Phys Chem Ref Data*. 1992;21(4):753-791. https://doi.org/10.1063/1.555914.

64. Tsang W, Herron JT. Chemical kinetic data base for propellant combustion. I. Reactions involving NO, NO_2, HNO, HNO_2, HCN and N_2O. *J Phys Chem Ref Data*. 1991;20:609-663. https://doi.org/10.1063/1.555890.

65. Tsang W. Chemical kinetic data base for combustion chemistry. Part 2. Methanol. *J Phys Chem Ref Data*. 1987;16(3):471-508. https://doi.org/10.1063/1.555802.

66. Tsang W, Hampson RF. Chemical kinetic data base for combustion chemistry. Part I. Methane and related compounds. *J Phys Chem Ref Data*. 1986;15(3):1087-1222. https://doi.org/10.1063/1.555759.

67. Manion JA, Huie RE, Levin RD, et al. NIST Chemical Kinetics Database, NIST Standard Reference Database 17, Version 7.0 (Web Version), Release 1.6.8, Data version 2015.09, National Institute of Standards and Technology, Gaithersburg, Maryland, 20899–8320. Published online 2013. http://kinetics.nist.gov/

68. Papp M, Valkó É, Turányi T, Evaluation of High-Temperature Gas Phase Rate Coefficients. Published 2020. https://k-evaluation.elte.hu/

69. Ruscic B, Bross DH, Active Thermochemical Tables (ATcT) Values Based on ver. 1.122g of the Thermochemical Network. Published Online 2019. http://atct.anl.gov

70. Sander SP, Finlayson-Pitts BJ, Friedl RR, et al. Chemical Kinetics and Photochemical Data for Use in Atmospheric Studies, Evaluation Number 14, JPL Publication 02–25. Published Online 2002. https://jpldataeval.jpl.nasa.gov/

71. Cox JD, Wagman DD, Medvedev VA. *CODATA Key Values for Thermodynamics*. Hemisphere Publishing Corp.; 1984.

72. Chase MW. *NIST-JANAF Themochemical Tables*. 4th ed. American Institute of Physics; 1998.

73. vom Lehn F, Cai L, Pitsch H. Sensitivity analysis, uncertainty quantification, and optimization for thermochemical properties in chemical kinetic combustion models. *Proc Combust Inst*. 2019;37(1):771-779. https://doi.org/10.1016/j.proci.2018.06.188.

SUPPORTING INFORMATION

Additional supporting information may be found online in the Supporting Information section at the end of the article.

How to cite this article: Kovács M, Papp M, Zsély IGy, Turányi T. Main sources of uncertainty in recent methanol/NOx combustion models. *Int J Chem Kinet*. 2021;53:884–900. https://doi.org/10.1002/kin.21490